13th International Symposium on Turbulence and Shear Flow Phenomena (TSFP13)
Montreal, Canada, June 25–28, 2024

STOCHASTIC MAP-BASED MODELING OF A LIFTED METHANE/AIR JET FLAME IN A VITIATED COFLOW

Tommy Starick
Chair of Numerical Fluid
and Gas Dynamics
BTU Cottbus-Senftenberg
D-03046 Cottbus, Germany
Tommy.Starick@b-tu.de

Heiko Schmidt
Chair of Numerical Fluid
and Gas Dynamics
BTU Cottbus-Senftenberg
D-03046 Cottbus, Germany
Heiko.Schmidt@b-tu.de

ABSTRACT

The present preliminary study investigates numerically a lifted methane/air jet flame in a vitiated coflow by means of the map-based, stochastic one-dimensional turbulence (ODT) model. The ODT model is efficient in terms of computational effort and provides nonetheless full-scale resolution along a notional line of sight crossing the turbulent reactive flow field. ODT uses a stochastic formulation for the turbulent advection and considers diffusion and reaction effects along the one-dimensional domain by temporally advancing deterministic evolution equations. In the considered Cabra burner configuration [Combust. Flame 143 491-506 (2005)], a jet flame issues from a central nozzle into a vitiated coflow of hot reaction products generated from an array of lean hydrogen/air flames. For the representation of the methane/air combustion, a reduced and detailed reaction mechanism with 19 and 53 species is used, respectively. Centerline profiles for mixture fraction, temperature and species mass fractions reveal reasonable agreement with the experimental data. Radial profiles of the lifted jet flame are also provided and compared to the existing measurements. Furthermore, scatter plots and two-dimensional visualizations of the jet flame are also given including an evaluation of the autoignition index to distinguish between autoignition and propagation driven reaction zones. The subtle interactions of the hot coflow with the cold unburnt jet flow are crucial for the entire reaction and autoignition process of the jet. Considering the reduced order and efficiency of the model, ODT is able to predict the key characteristics and reasonably matches the experimental measurements.

INTRODUCTION & ODT FORMULATION

Recirculation burners are widely used in industry and are subject to increasingly strict requirements for lower pollutant emissions, higher efficiency and wider fuel and operational flexibility. The numerical investigation of this type of burner is complex due to the recirculation of hot combustion products. Vitiated coflow burners instead consist of a lifted jet flame in an environment of hot combustion products and exhibit similar characteristics for chemical kinetics, heat transfer and molecular transport as recirculation burners, while avoiding their complex recirculating fluid mechanics, as detailed in the experimental measurements of Cabra *et al.* (2005).

In this study, we address the numerical investigation of a lifted methane/air jet flame in a vitiated coflow by means of the one-dimensional turbulence (ODT) model. For this application, a cylindrical and temporal ODT formulation is used, as can be reviewed in Lignell *et al.* (2018).

In an effort to resolve all relevant scales and still be able to achieve realistic Reynolds number flows in numerical simulations, Kerstein (1999) introduced the one-dimensional turbulence (ODT) model. ODT is an efficient alternative to direct numerical simulations (DNS) without compromising on the full-scale resolution. ODT uses a stochastic and map-based formulation for the representation of the turbulent advection. The diffusion and reaction kinetics along the one-dimensional domain are considered by temporally advancing deterministic evolution equations. In comparison to averaged or filtered simulation approaches such as Reynolds-averaged Navier-Stokes (RANS) or large eddy simulations (LES), ODT incorporates molecular processes (e.g. chemical reactions and diffusive transport) without introducing additional approximations or modeling assumptions.

The effects of 3-D turbulence are incorporated in ODT by the implementation of so-called stochastic eddy events. These eddy events directly model the characteristics of turbulent transport on the fluid properties along the simulated 1-D domain. Every eddy event perturbs any of the property fields by the application of a triplet map.

A triplet map is a measure preserving transformation rule which ensures the continuity of advected fields and leads to a steepening of local property gradients (Lignell *et al.*, 2018; Ashurst & Kerstein, 2005). It takes a line segment $[r_0, r_0 + l]$ with a randomly determined eddy location r_0 and size l, shrinks it to a third of its original length, and then places three

copies of this on the original domain. The middle copy is reversed. Review Lignell *et al.* (2018) for the features of the triplet map in the cylindrical ODT formulation.

Eddy events are sampled in time as a marked Poisson process by means of presumed Probability Density Functions (PDFs) for eddy locations r_0 and eddy sizes l. This procedure is able to replicate the statistics of turbulent flows on average by oversampling the number of events modelling the turbulent transport, and maintaining a target mean acceptance probability of eddy events, as reviewed in McDermott (2005) and Lignell *et al.* (2018). The acceptance probability of a particular eddy in a given sampling time interval Δt_{sample} is determined by the calculation of a rate λ of the eddy candidate.

The eddy rate λ, which is given by the expression in Eq. 1, depends on r_0, l and the eddy event time scale τ. The latter is proportional to the difference between the available kinetic energy E_{kin} in the eddy range and an energetic viscous penalty E_{vp} for the suppression of too small eddies, following Lignell *et al.* (2018). The latter term has no significant influence on the statistical results, but proves to be beneficial for the performance of the model.

$$\lambda(r_0, l, \tau) \equiv \frac{C}{l^2 \tau} \sim C\left(E_{kin} - Z E_{vp}\right) \tag{1}$$

C and Z are dimensionless ODT model parameters which are initially calibrated to an individual flow configuration and then kept constant.

ODT lacks large scale coherent information due to its reduced dimensionality. The eddy sampling process may occasionally accept an unphysically large eddy in the initial phase, which may unfavorably affect the turbulent transport. This can be avoided in ODT by using a large eddy suppression mechanism. This suppresses eddies which have an eddy event time scale proportionally larger than the elapsed simulation time t. In general, eddies are only implemented if the following condition

$$\tau \leq \beta t \tag{2}$$

is satisfied, where β is another dimensionless ODT model parameter which must be determined beforehand (Lignell *et al.*, 2018).

Eddies are sampled sequentially in time. After an eddy is implemented, a deterministic catch up process of diffusive-reactive transport equations takes place up to the physical time at which the eddy was deemed to be implemented. In an open system configuration, as given by the investigated lifted jet flame in this work, the deterministic advancement is governed by integral conservation laws following a Lagrangian ODT formulation, as detailed in Lignell *et al.* (2018).

The integral expressions for conservation of mass, momentum, and energy are listed in the following. The mass conservation equation is given by following equation.

$$\frac{\mathrm{d}}{\mathrm{d}t} \int \rho r \mathrm{d}r = 0 \tag{3}$$

Here, ρ stands for the density of the gas mixture, which is correlated with the pressure, temperature and molecular weight of the mixture given by the ideal gas law.

$$P = \rho R_u T \sum_k \frac{Y_k}{M_k} \tag{4}$$

In this relation, P stands for the thermodynamic pressure, which remains temporally and spatially unchanged in the open jet flame configuration. Furthermore, R_u is the universal gas constant, T is the temperature of the gas mixture and Y_k and M_k are the different mass fractions and molecular weights of the k species forming the gas mixture, respectively. The species conservation equation is given by:

$$\frac{\mathrm{d}}{\mathrm{d}t} \int \rho Y_k r \mathrm{d}r = -\int \frac{1}{r} \frac{\partial}{\partial r} \left(\rho V_k Y_k\right) r \mathrm{d}r + \int \dot{w}_k r \mathrm{d}r \tag{5}$$

Here, V_k are the species diffusion velocities, which require the same modelling approximations as in any reactive DNS. Similarly, $\dot{w}_k$ are the species reaction rates provided by an imported reaction mechanism at specified thermodynamic conditions.

For the conservation of momentum, we assume dominance of radial transport and use the gradient of scalar modeled shear stresses as those responsible for the diffusion of momentum in the system, as in Lignell *et al.* (2018).

$$\frac{\mathrm{d}}{\mathrm{d}t} \int \rho u_i r \mathrm{d}r = \int \frac{1}{r} \frac{\partial}{\partial r} \left(r \mu \frac{\partial u_i}{\partial r}\right) r \mathrm{d}r \tag{6}$$

In the momentum conservation equation, u_i stands for the three velocity components in the cylindrical system and μ is the dynamic viscosity of the gas mixture. Finally, the energy conservation in the open system is being represented by the conservation of enthalpy h in a zero Mach number limit approximation.

$$\begin{aligned} \frac{\mathrm{d}}{\mathrm{d}t} \int \rho h r \mathrm{d}r = &-\int \frac{1}{r} \frac{\partial}{\partial r} \left(\rho V_k Y_k h_k\right) r \mathrm{d}r \\ &+ \int \frac{1}{r} \frac{\partial}{\partial r} \left(r \lambda_t \frac{\partial T}{\partial r}\right) r \mathrm{d}r \end{aligned} \tag{7}$$

In this equation, h_k stands for the sensible enthalpy of each k^{th} species and λ_t is the thermal conductivity of the mixture.

The deterministic temporal advancement of Eq. 3-7 is realized by means of a finite volume method (FVM) using a first order time integration. For the studied lifted methane/air jet flame, an implicit time-integration of Eq. 3-7 considering the diffusive flux terms calculated at the beginning of the time step as constants in order to remediate the potentially restrictive CFL condition due to stiff chemistry initiated by the species chemical reaction source term is performed. However, this converts the time integration in Eq. 6-7, into an explicit Euler method.

The density obtained after time stepping the enthalpy and species conservation equations (Eq. 7 and 5) is calculated by means of Eq. 4 at the new mixture composition and temperature. After the density is updated, mass conservation is enforced by a conservative remeshing of the grid following the application of the mass conservation equation (Lignell *et al.*, 2013). The fluid thermophysical properties are calculated using the Cantera software suite, see Goodwin (2002) for further details.

CONFIGURATION

The Cabra burner configuration (Cabra *et al.*, 2005) consists of a lifted methane/air jet flame in a vitiated coflow of hot combustion products generated from an array of lean H_2/air flames. For all conducted ODT simulations, the initial condition of the coflow consists of an uniform velocity profile of 5.4 m/s and

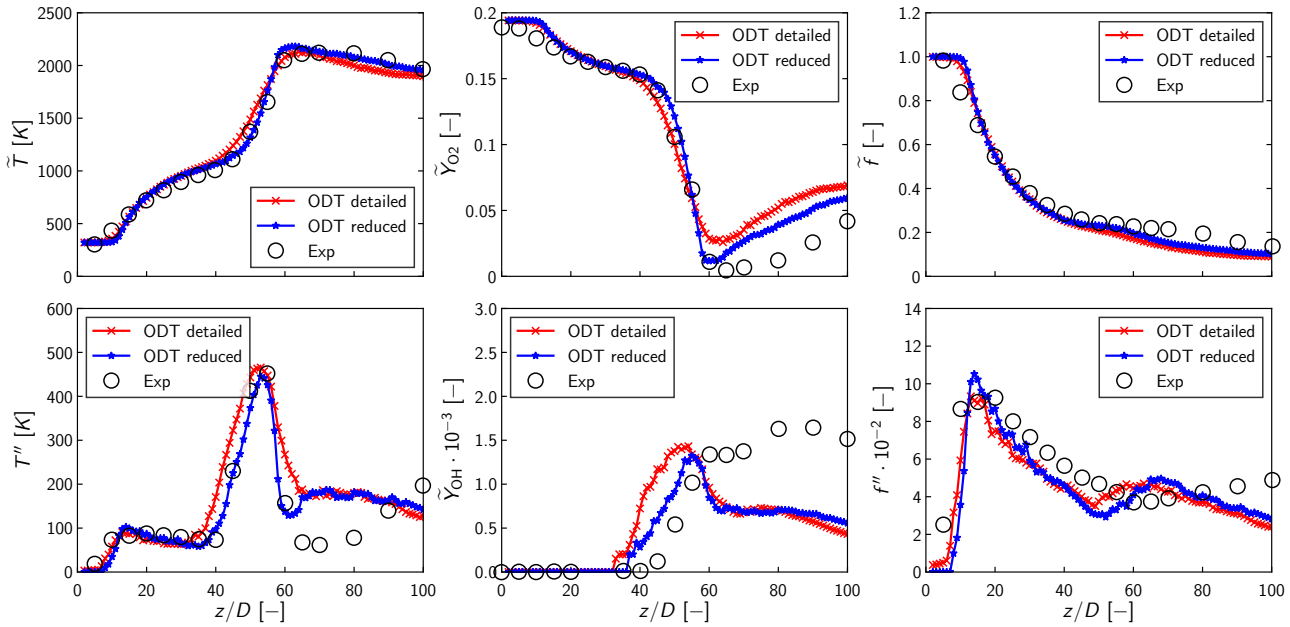

Figure 1: Centerline profiles of Favre-averaged temperature ($\tilde{T}$ and fluctuations T''), species mass fractions (Favre-averaged oxygen mass fraction $\tilde{Y}_{O2}$ and Favre-averaged hydroxyl radical mass fraction $\tilde{Y}_{OH}$), and mixture fraction ($\tilde{f}$ and fluctuations f'') from ODT simulations using a reduced and detailed reaction mechanism for the representation of the methane/air combustion. ODT results are compared to the experimental measurements of Cabra *et al.* (2005) (Exp).

a constant temperature of 1350 K. The cold jet is initialized with a fixed temperature of 320 K and an instantaneous velocity profile generated from ODT pipe flow simulations with a bulk velocity of 100 m/s. The diameter D and composition of the jet and coflow are given in Table 1. For the representation of the chemical reactions, the detailed GRI-Mech 3.0 mechanism (Smith *et al.*, 1999) with 53 species and 325 reactions and a reduced reaction mechanism (Lu & Law, 2008) with 19 species and 15 reactions is used.

Table 1: Initial conditions of the jet and coflow.

-	Jet	Coflow
D (mm)	4.57	100
u (m/s)	100	5.4
T (K)	320	1350
$X_{\mathrm{CH_4}}$	0.33	0.0003
$X_{\mathrm{O_2}}$	0.15	0.12
$X_{\mathrm{N_2}}$	0.52	0.73
$X_{\mathrm{H_2O}}$	0.0029	0.15
X_{OH} (ppm)	0.0	200
$X_{\mathrm{H_2}}$ (ppm)	100	100

The ODT results are intended to be compared with the stationary spatially developing round jet flame measurements of Cabra *et al.* (2005). However, the applied ODT formulation only solves for a radial location r and time t. Consequently, a transformation between time and their corresponding downstream position z is required. This is implemented by a downstream advection of the ODT line with an instantaneous bulk velocity $\bar{u}$.

$$z(t) = z(t_0) + \int_{t_0}^{t} \bar{u}(t')dt' \tag{8}$$

Here, $z(t_0)$ marks the starting position. The bulk velocity $\bar{u}$ is calculated by the sum of the free-stream (coflow) velocity and the ratio of integrated momentum flux to integrated mass flux, as detailed in Echekki *et al.* (2001)

$$\bar{u}(t) = u_\infty + \left.\frac{\int_{-\infty}^{\infty} \rho(u-u_\infty)^2 r dr}{\int_{-\infty}^{\infty} \rho(u-u_\infty) r dr}\right|_t \tag{9}$$

For the mixture fraction, the definition of Bilger *et al.* (1990) is used.

$$f = \frac{2(Y_\mathrm{C} - Y_{\mathrm{C},2})/M_\mathrm{C} + (Y_\mathrm{H} - Y_{\mathrm{H},2})/2M_\mathrm{H} - (Y_\mathrm{O} - Y_{\mathrm{O},2})/M_\mathrm{O}}{2(Y_{\mathrm{C},1} - Y_{\mathrm{C},2})/M_\mathrm{C} + (Y_{\mathrm{H},1} - Y_{\mathrm{H},2})/2M_\mathrm{H} - (Y_{\mathrm{O},1} - Y_{\mathrm{O},2})/M_\mathrm{O}} \tag{10}$$

In this relation, M denotes the elemental masses and Y the mass fractions of carbon (C), hydrogen (H), and oxygen (O). The subscripts 1 and 2 mark the jet and the coflow, respectively.

RESULTS

ODT simulations with a reduced and detailed mechanism were conducted and compared to the experimental measurements of Cabra *et al.* (2005). In Figure 1, centerline profiles

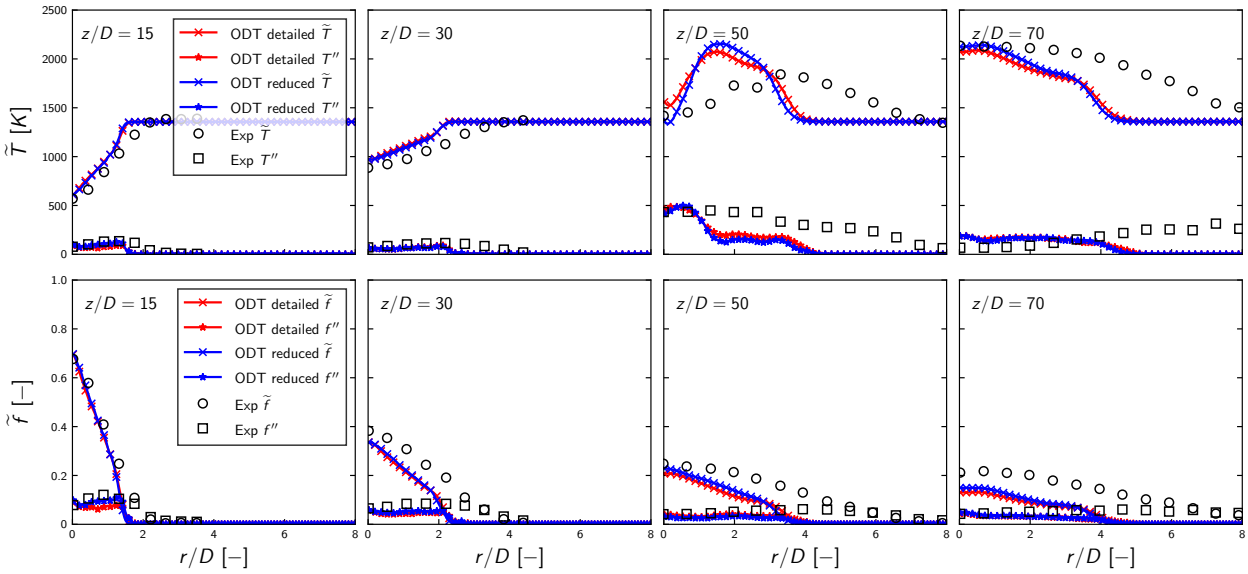

Figure 2: Radial profiles of Favre-averaged temperature ($\tilde{T}$ and fluctuations T'') and Favre-averaged mixture fraction ($\tilde{f}$ and fluctuations f'') from ODT simulations using a reduced and detailed mechanism for the representation of the methane/air combustion. ODT results are compared to the experimental measurements of Cabra *et al.* (2005) (Exp).

of the Favre-averaged species mass fractions, Favre-averaged temperature, Favre-averaged mixture fraction and their corresponding fluctuations are given. In all centerline plots, the red and blue curves show results from ODT simulations with a detailed and reduced reaction mechanism, respectively. The measurement data from Cabra *et al.* (2005) is indicated by round black markers. The Favre-averaging of the ODT results is based on an ensemble size of 400 realizations. For all shown results, the ODT model parameters C and Z in Eq. 1 are taken as $C = 18$ and $Z = 400$, which are the same model parameters used in the investigations of a round jet flame with a likewise cylindrical formulation done by Lignell *et al.* (2018). The large eddy suppression in the initial phase of the simulation is using a fixed model parameter of $\beta = 1.17$.

The initial phase up to $z/D \approx 40$ is dominated by non-reactive mixing of the cold jet and the hot coflow. This is followed by the flame stabilization phase. Here, a strong temperature rise, rapid oxygen consumption, hydroxyl radical production and peak in the temperature fluctuations takes place. The ODT results for both reaction mechanisms are in reasonable agreement with the experimental data. This includes a correct representation of the mixing in the initial phase and an accurate capture of the combustion process, which is denoted by a rapid temperature rise and oxygen mass fraction drop. ODT also almost captures the trend and magnitude of the Favre fluctuations from the experimental measurements.

In addition to the centerline profiles, Fig. 2 shows the radial profiles of the Favre-averaged temperature, Favre-averaged mixture fraction and their corresponding fluctuations. Similar to the centerline profiles, the red and blue curves show results from ODT simulations with a detailed and reduced reaction mechanism, respectively. The experimental data for the Favre-averaged value and their corresponding fluctuation is indicated by round black markers and square black markers, respectively. In the initial phase with non-reactive mixing of the cold and hot coflow ($z/D = 15$ and $z/D = 30$), the ODT results for both reaction mechanisms is are in reasonable agreement with the experimental measurements. For positions further downstream ($z/D = 50$ and $z/D = 70$), deviations between the ODT results and the experimental measurements can be observed. These deviations are probably caused by the used approximation for the determination of the downstream position given by Eq. 8 and 9. In contrast to the centerline, the calculation of the downstream position based on a radially uniform bulk velocity for every time step is presumably not completely appropriate for the shear region between cold jet and hot coflow. At this point, using a spatial ODT formulation (Lignell *et al.*, 2018) could represent a more realistic advection of the ODT line in downstream direction.

Fig. 3 shows scatter plots of temperature versus mixture fraction and OH mass fraction versus mixture fraction at four different downstream positions. These figures are obtained by showing either the values of temperature and mixture fraction or OH mass fraction and mixture fraction for each grid cell at a given time (fixed axial position). For a better visibility, only 25 realizations out of the full ensemble size of 400 simulations are shown. In each plot, the dotted vertical line represents the stoichiometric mixture fraction of $f_s = 0.17$ and the dashed line non-reacting conditions (pure mixing). The solid black line in the scatter plots for temperature versus mixture fraction marks equilibrium. At an axial position of $z/D = 15$, the state is characterized by pure mixing and no reactions are taking place. The state of complete equilibrium is reached at a downstream position of $z/D = 70$. In the scatter plots at the downstream position of $z/D = 40$ and $z/D = 50$, some data points already reached equilibrium and others are still in a condition of pure mixing. The scatter plots are showing that ODT captures the key combustion characteristics and is able to reproduce the scatter plots of the experimental measurements of Cabra *et al.* (2005) (not shown here).

Fig. 4 (a,c,d) shows two-dimensional renderings of the Favre-averaged temperature, mixture fraction and heat release rate, respectively. Considering the reduced dimensionality of ODT, the generation of two-dimensional renderings of the

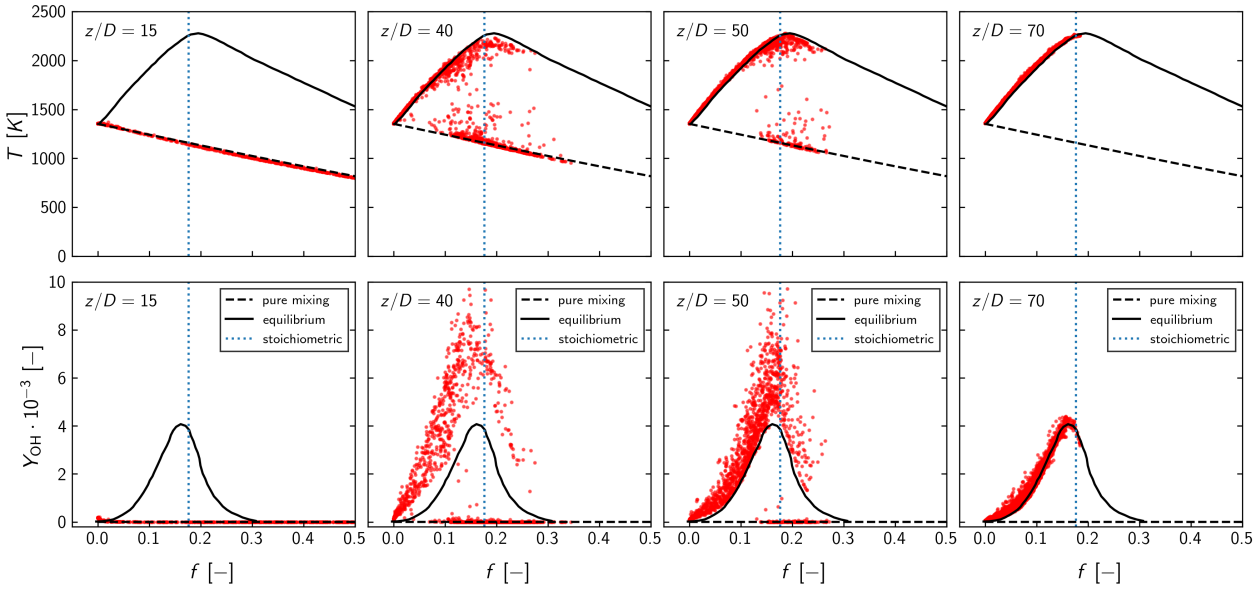

Figure 3: Scatter plots at four different downstream positions from cylindrical ODT simulations using a detailed reaction mechanism. The scatter plots are showing the instantaneous distribution of temperature versus mixture fraction and OH mass fraction versus mixture fraction.

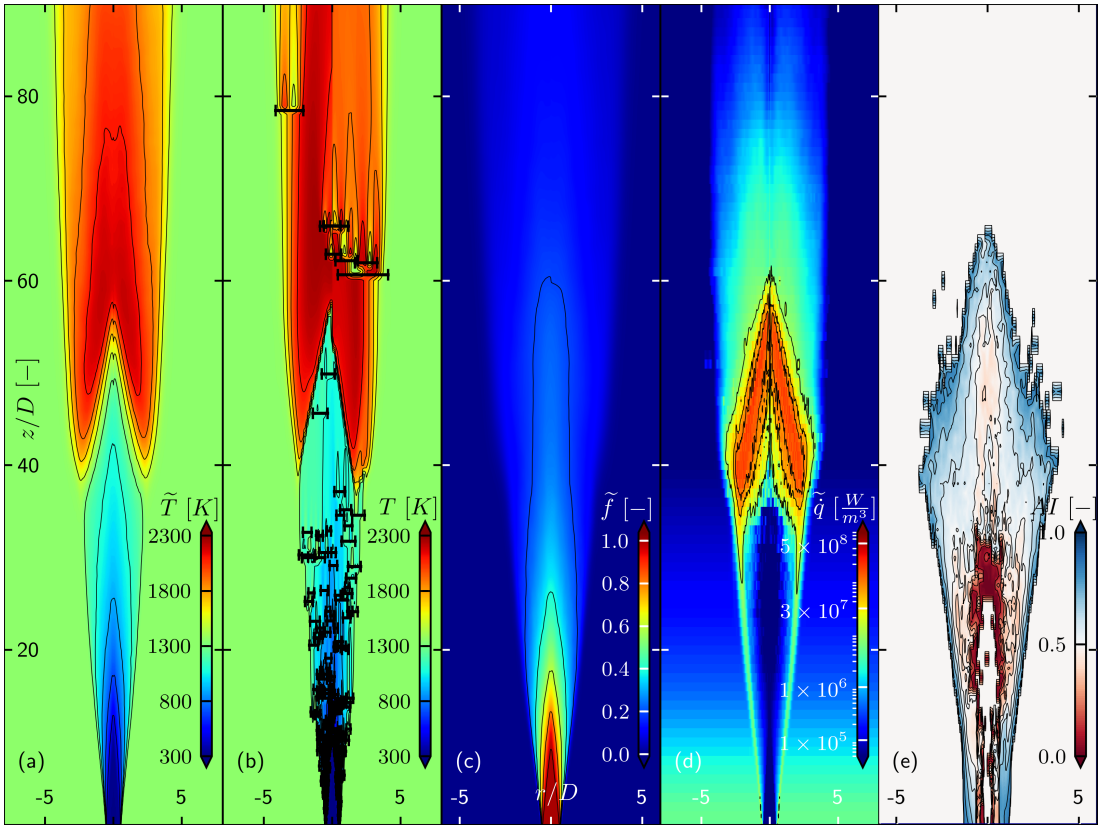

Figure 4: Two-dimensional renderings of the Favre-averaged temperature (a), mixture fraction (c), and heat release rate (d) from ODT simulations using a detailed methane/air reaction mechanism. Figure (b) visualizes the temperature distribution of the lifted methane/air jet flame from a single ODT realization. The black bars mark the stochastically sampled and implemented eddy events. Figure (e) illustrates the mean autoignition index (AI) averaged over all ODT simulations.

lifted jet flame is a remarkable outcome of the model. In Fig. 4 (b), the temperature distribution with visualized eddy events from a single ODT realization is given. The black bars mark the implemented eddy events, which incorporate the effects of three-dimensional turbulence into ODT.

The autoignition index (AI) allows a distinction between autoignition and propagation driven reaction zones, as detailed in Schulz *et al.* (2017). The definition of the autoignition is based on a reaction rate flux analysis of the HO_2 chemistry. In the detailed GRI-Mech 3.0 mechanism (Smith *et al.*, 1999) with 53 species and 325 reactions, the reactions responsible for consumption of HO_2 and important for distinguishing between autoignition and propagation driven reaction zones is through the following two reactions.

$$\mathrm{HO_2 + H \longleftrightarrow OH + OH} \qquad \left[R46\right]$$

$$\mathrm{HO_2 + OH \longleftrightarrow H_2O + O_2} \qquad \left[R287\right]$$

The autoignition index is given by following definition (Schulz *et al.*, 2017).

$$AI = \left| \frac{\dot{w}_{HO_2}^{R287}}{\dot{w}_{HO_2}^{R287} + \dot{w}_{HO_2}^{R46}} \right| \tag{11}$$

Here, $\dot{w}_{HO_2}^{R287}$ stands for the contribution of reaction 287 to the reaction rate of HO_2 in the detailed reaction mechanism. Similarly, $\dot{w}_{HO_2}^{R46}$ is the contribution of reaction 46 to the reaction rate of HO_2.

Fig. 4 (e) visualizes the mean autoignition index. The blue (AI $>$ 0.5) or red regions (AI $<$ 0.5) mark autoignition or propagation dominated reaction zones, respectively. Here, propagation is predominant in the core of the flame and autoignition in the transition region to the hot coflow. In comparison to the instantaneous AI results from a 3-D LES simulation provided by Schulz *et al.* (2017) (not shown here), the ODT results reveal similar positions of autoignition and propagation driven reaction zones. Considering the reduced order of the ODT model, the possibility of providing information about the distribution of the autoignition index and the reasonable agreement with the findings of Schulz *et al.* (2017) are remarkable accomplishments of ODT.

CONCLUSIONS

Preliminary ODT simulation results for a lifted methane/air jet flame configuration in an environment of hot combustion products were presented. A cylindrical and temporal ODT formulation with a reduced and detailed reaction mechanism was used and compared to experimental measurements of Cabra *et al.* (2005). The detailed mechanism uses 53 species and 325 reactions and the reduced mechanism 19 species and 15 reactions. The comparison of the centerline profiles to the experimental data revealed a reasonable agreement for both reaction mechanism. ODT is able to reproduce the Favre-averaged centerline profiles and their corresponding fluctuations. Furthermore, the radial profiles for pure mixing (z/D <30) were in a reasonable agreement with the experiments. For positions further downstream (z/D >30), the ODT results revealed deviations to the experimental data. The scatter plots show that ODT is able to capture the key combustion characteristics and reasonably match the experimental measurements. The two-dimensional visualizations of the lifted methane/air jet flame demonstrate the capabilities of ODT in providing two-dimensional information from a reduced order simulation. In general, the results obtained indicate that ODT is able to capture the important combustion features of the investigated lifted methane/air jet flame in a vitiated coflow. Considering the reduced order of the model, ODT is an efficient and scale resolving turbulence model for reactive jet flame simulations.

ACKNOWLEDGEMENTS

The authors thank for funding by the BTU Graduate Research School (Conference Travel Grant).

REFERENCES

Ashurst, Wm. & Kerstein, A 2005 One-dimensional turbulence: Variable-density formulation and application to mixing layers. *Physics of Fluids* **17**.

Bilger, R.W., S.H., Stårner & R.J., Kee 1990 On Reduced Mechanisms for Methane-Air Combustion in Nonpremixed Flames. *Combustion and Flame* **80**, 135–149.

Cabra, R., Chen, J.-Y., Dibble, R. W., Karpetis, A. N. & Barlow, R. S. 2005 Lifted methane-air jet flames in a vitiated coflow. *Combustion and Flame* **143**, 491–506.

Echekki, T., Kerstein, A. & Dreeben, T. 2001 One-Dimensional Turbulence Simulation of Turbulent Jet Diffusion Flames: Model Formulation and Illustrative Applications. *Combustion and Flame* **125**, 1083–1105.

Goodwin, D 2002 *Cantera C++ User's Guide*. California Institute of Technology.

Kerstein, A. 1999 One-dimensional turbulence: model formulation and application to homogeneous turbulence, shear flows, and buoyant stratified flows. *Journal of Fluid Mechanics* **392**, 277–334.

Lignell, D, Kerstein, A, Sun, G & Monson, E 2013 Mesh adaption for efficient multiscale implementation of One-Dimensional Turbulence. *Theoretical and Computational Fluid Dynamics* **27** (3-4), 273–295.

Lignell, D., Lansinger, V., Medina M., Juan A., Klein, M., Kerstein, A., Schmidt, H., Fistler, M. & Oevermann, M. 2018 One-dimensional turbulence modeling for cylindrical and spherical flows: model formulation and application. *Theoretical and Computational Fluid Dynamics* **32**, 495–520.

Lu, T.F. & Law, C.K. 2008 A criterion based on computational singular perturbation for the identification of quasi steady state species: A reduced mechanism for methane oxidation with NO chemistry. *Combustion and Flame* **154**, 761–774.

McDermott, R. 2005 Towards One-Dimensional Turbulence Subgrid Closure for Large-Eddy Simulation. PhD thesis, University of Utah.

Schulz, O., Jaravel, T., Poinsot, T., Cuenot, B. & Noiray, N. 2017 A criterion to distinguish autoignition and propagation applied to a lifted methane–air jet flame. *Proceedings of the Combustion Institute* **36** (2), 1637–1644.

Smith, G. P., Golden, D. M., Frenklach, M., Moriarty, N. W., Eiteneer, B., Goldenberg, M., Bowman, C. T., Hanson, R. K., Song, S., Gardiner, W. C., Lissianski, V. V. & Qin, Z. 1999 `http://www.me.berkeley.edu/gri_mech/`. *Tech. rep.* .